International Journal of Academic Engineering Research (IJAER)
ISSN: 2643-9085
Vol. 5 Issue 3, March - 2021, Pages: 80-87

Reactions at the Electrode/Electrolyte Interface Of All-Solid-State Lithium Batteries Incorporating Li–M (M = Sn, Si) Alloy Electrodes and Sulfide-Based Solid Electrolytes

Jurabek Abdiyev[1],Sadulla Saydullayev[1], Elyor G'aybulloyev[2], Sherzod Yarashev[2*], Bekzod Erkinov[2]

[1]Physical-technical Institute of NPO "Physics – Sun" of Uzbekistan Academy of Sciences Uzbekistan, Tashkent, Chingiz Aitmatov street 2B.

[2]Tashkent University of Information Technologies named after Muhammad al-Khwarizmi, Uzbekistan, Tashkent, Amir Temur street 108.

Corresponding author: sherzodyarashev1997@gmail.com (Sh. Yarashev)

Abstract: *Reactions at the electrode/electrolyte interface of all-solid-state lithium batteries were studied for combinations of sulfide-based solid electrolytes with various $Li_{4-x}Ge_{1-x}P_xS_4$ and Li_y-M (M = Sn, Si) alloys as the negative electrodes, using ac impedance, X-ray diffraction and energy-dispersive X-ray spectroscopy. The solid electrolyte at the interfacial region was found to decompose with the application of a current through the cells, resulting in the formation of a solid electrolyte interphase (SEI) layer. Resistivity changes at the interface varied depending on the electrolyte composition and the redox potential (vs. Li/Li^+) of the negative electrode material. Lower resistances were observed with lower Ge contents in the solid electrolyte and the use of a Li–M alloy with a higher redox potential due to the formation of an electrochemically stable SEI layer during battery operation. In contrast, a combination of higher Ge content and an alloy with a lower redox potential led to a rapid increase in the SEI resistance and increase in its thickness. The presence of a Li–P–S compound with low ionic conductivity in the interfacial region was found to be related with the increase of interfacial resistance, leading to poor cycling characteristics. The formation of a suitable SEI layer is an important factor in the future development of all-solid-state batteries and this study serves to clarify the relationships between the formation of the SEI phase, the redox potential of the electrode and the sulfide-based solid electrolyte composition.*

Keywords: Interface resistance, Sulfide-based solid electrolyte, Electrolyte decomposition.

1. INTRODUCTION.

A key factor in designing electric or plug-in hybrid vehicles and energy storage devices for wind or solar power generation is the development of battery technologies that allow higher energy and power densities with suitable margins of safety [1,2]. With regard to both safety and reliability, all-solid-state lithium batteries incorporating non-flammable solid electrolytes are one of the most promising candidates. The most important component of such batteries is the electrolyte and one class of potential inorganic solid electrolytes, which exhibit high ionic conductivities, are sulfide-based materials. As an example, $Li_{10}GeP_2S_{12}$ ($Li_{3.35}Ge_{0.35}P_{0.65}S_4$) has an ionic conductivity of 1.2×10^{-2} S cm^{-1} at room temperature, which is comparable to the values obtained using organic electrolytes. The sulfide-based solid electrolyte family also provides a wide potential window with a high resistance to decomposition of up to ~5 V (vs. Li/Li^+), which is suitable for use in all-solid-state batteries [3,4].

However, challenges related to fabricating electrochemical inter-faces with a suitable degree of contact between the electrode and the electrolyte prevent the practical application of these materials in batteries. In the case of conventional liquid electrolyte-based batteries, the entire surface of the electrode is covered, which enables the electro-chemical lithium (de)intercalation reaction to proceed readily over the whole interfacial region. In contrast, it is difficult to achieve close con-tact with a solid/solid interface in all-solid-state batteries because of the hard, brittle characteristics of inorganic solids [5]. Consequently, the resulting smaller electrode reaction area increases the interface resistance. It is therefore important to control the resistance of the electrode/solid electrolyte interface in all-solid-state batteries.

Previous studies have examined the interfacial reactions of all-solid-state batteries using sulfide-based solid electrolytes belonging to the thio-LISICON family. These studies examined batteries incorporating $Li_{3.25}Ge_{0.25}P_{0.75}S_4$ as the solid electrolyte with a Li–Al alloy as the negative electrode and found good cycling characteristics due to the formation of an interfacial phase at the electrode/electrolyte boundary during charge–discharge measurements [5,6]. When a current is applied to an all-solid-state battery, a solid electrolyte interphase (SEI) layer is formed at the interface between the thio-LISICON solid electrolyte and the electrode. The SEI layer is composed of the decomposition products of the solid electrolyte. Although this SEI layer improves the contact conditions at the electrode/electrolyte interface and reduces the charge-transfer resistance, the interfacial resistance increases with the growth of the SEI layer during charge–discharge cycling because of the lower ionic conductivity of this layer compared to the electrolyte. In order to control the formation of the SEI layer at the interface, it is important to select an appropriate combination of solid electrolyte and electrode materials [5]. However, even though the anode and the solid electrolyte

interface play key roles in the battery performance there is little information available concerning the effects of various combinations of materials and the associated decomposition processes at the negative electrode/electrolyte interface [5,6].

In the present study, the reactions at the negative electrode/electrolyte interface were examined using sulfide-based solid electrolytes, including the new electrolytes: $Li_{4-x}Ge_{1-x}P_xS_4$ (LGPSx), and employing high capacity Li–M (M = Sn, Si) alloy negative electrodes [3,7]. Recent studies on the germanium based sulfide electrolyte clarified the extremely high ionic conductivity above 10^{-2} S cm^{-1} at room temperature for the near the thio-LISICON composition of $Li_{3.75}Ge_{0.25}P_{0.75}S_4$, however clarification of the electrochemical stabilities of these materials with a combination of anode alloys is necessary. These alloys are useful since tin has a theoretical capacity of 990 mAh g^{-1}, which is approximately 2.7 times that of a carbon negative electrode (372 mAh g^{-1}) [8], while the high ductility of Sn might allow more intimate contact at the solid/solid interface. In addition, the higher lithium diffusion rate in Sn compared to that in Al might improve the discharge rate characteristics of the system [9,10]. Silicon is another well-known negative electrode material and has a high theoretical capacity of 4200 mAh g^{-1}. The resulting interfacial phase formation and electro-chemical properties were examined by evaluating the interfacial resistance and by observing the interfacial region using X-ray diffraction (XRD) and energy-dispersive X-ray spectroscopy (EDX). The relation-ships between the SEI phase formation, the electrode redox potentials, the sulfide-based solid electrolyte composition and the interfacial resistance were thus investigated. Furthermore, we constructed a comparative model of the SEI layers in the all-solid-state batteries by purposefully adding Li_2S, P_2S_5 or GeS_2, which may be present at the in-terface as decomposition products. The effects and behavior of the model SEI layers during battery reaction were also investigated by the same electrochemical techniques as the pristine samples.

2. EXPERIMENTAL.

Three sulfide-based solid electrolytes were used: $Li_{3.25}Ge_{0.25}P_{0.75}S_4$, $Li_{3.35}Ge_{0.35}P_{0.65}S_4$ and $Li_{3.5}Ge_{0.5}P_{0.5}S_4$, where the $Li_{4-x}Ge_{1-x}P_xS_4$ compositions in the ternary Li_2S–GeS_2–P_2S_5 system are represented by the formula LGPSx. The synthesis processes by which these solid electrolytes were obtained have been described elsewhere [3,7,11]. Each of these solid electrolytes was ground using a vibrating mill prior to the cell experiments.

Symmetric cells with the configuration Li–M alloy/solid electrolyte/ Li–M alloy (M = Sn, Si) were used for the charge–discharge experiments. Each cell consisted of a polyethylene terephthalate (PET) cylinder with an inner diameter of 10 mm. A solid electrolyte sample of approximately 100 mg was pressed into a pellet at 147 MPa, following which, Sn powder (99.8%, 325 mesh, Alfa Aesar) was pressed onto one side of the electrolyte pellet at 184 MPa and Li foil (0.6 mm thick, 6 mm diameter) was subsequently pressed onto the Sn layer at 9.2 MPa. Both electrodes had the same configuration, thus forming a symmetrical cell. Cells using a Li–Si alloy were also constructed via the same procedure but using Si powder (99.9%, 350 mesh, Nilaco) as the negative electrode material. Several alloy compositions with different Li/M (M = Sn, Si) ratios were examined to determine the relationship between the electrode redox potentials (vs. Li/Li^+) and the decomposition reactions. In these trials, the alloy compositions were varied by changing the ratios of Sn or Si to lithium metal in the electrodes. Charge–discharge data were obtained from the symmetric cells by applying a constant current of 1.38 mA cm^{-2} for 20 min, following which the same amount of current was applied but in the opposite direction. After each cycle of the charge–discharge process, the ac impedance of the cell was measured. All the electrochemical experiments were carried out at room temperature (25 °C). The resistances of the symmetrical cells were measured by the ac impedance method over an applied frequency range of 1 Hz to 1 MHz, using a frequency response analyzer (Solartron 1260) connected to an electrochemical interface (Solartron 1287). The software packages ZPLOT and ZVIEW were used for the measurements and the analyses, respectively [12].

The electrolyte layers were removed from the cells following the resistance measurements and the electrolyte surfaces were examined by XRD (Rigaku Smartlab) with CuKα radiation. The cross-sections of electrolyte samples were cut by ion-milling, and the surface regions of the electrolytes were also analyzed using EDX (EDX, Genesis 4000).

3. RESULTS AND DISCUSSION.

3.1. EFFECT OF ELECTROLYTE COMPOSITION.

Fig. 1 presents a typical example of the plots obtained from ac impedance measurements during charge–discharge cycling. The impedance of symmetrical cells has previously been described as the combination of two components, the high-frequency and low-frequency regions, which correspond to the SEI resistance (R_{SEI}) and charge-transfer resistance (R_{CT}), respectively [6]. In the obtained plots, a distinct semicircle at high-frequency regions around 100 kHz with a capacitance value of 10^{-7} to 10^{-9} F cm^2 represents the interfacial reaction at the anode/inorganic solid electrolyte [5,13]. The SEI resistance value of each cycle was calculated using this semicircle. The equivalent circuit used for the fitting of the impedance data was com-posed of a combination of the electrolyte and the electrode, R_{b+g}, and two R//CPE (constant phase element) circuits that correspond to the SEI layer and the charge-transfer components, respectively [6]. As reported in previous studies for other electrode/electrolyte systems [5, 6]. It is evident from this figure that the high-frequency semicircles be-came larger with cycling, indicating an increase in the resistivity caused by the continued formation of the SEI.

Fig. 2 summarizes the effects of cycling on the SEI resistance values of symmetric cells incorporating the three types of electrolytes and $Li_{4.4}Sn$ electrodes. Prior to cycling, the resistance values of the SEI re-gions were 48, 41 and 160 Ω for the cells using LGPS0.5, LGPS0.65 and LGPS0.75, respectively. In the initial state, there were no significant differences in the SEI resistivity values due to the cell compositions. How-ever, clear differences in the SEI resistance variations were observed during cycling. The resistance of the LGPS0.75 cell decreased following the 1st cycle and then slightly increased during subsequent cycles, how-ever the resistance value did not exceed 250 Ω. This behavior was similar to that of the symmetric cell composed of Li–Al/ $Li_{3.25}Ge_{0.25}P_{0.75}S_4$/ Al–Li, indicating the formation of a stable SEI layer at the interface [5, 6]. In contrast, a considerable increase is seen in the SEI resistance values of the cells incorporating LGPS0.65 and LGPS0.5 throughout the electro-chemical cycling. The SEI resistivity of these specimens continuously increased, reaching 458 and 1217 Ω after 20 cycles, respectively.

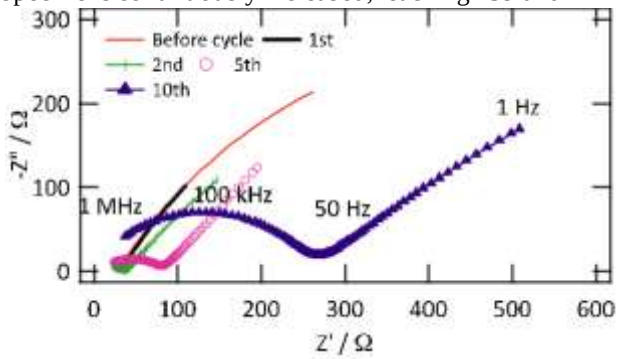

Fig. 1. Typical ac impedance plots for the $Li_{0.4}Sn$ alloy/LGPS0.5/$Li_{0.4}Sn$ alloy cell.

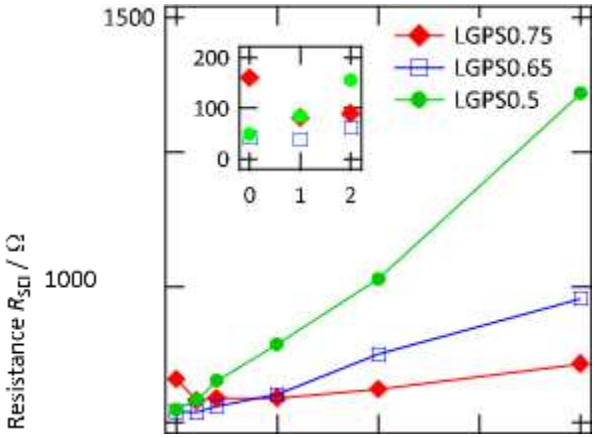

Fig. 2. Variations in SEI resistance with cycling for cells incorporating different sulfide-based solid electrolytes.

Table 2

Redox potentials of the negative electrode materials used in the present study.

Negative materials	Li_y–Sn alloy					Li_y–Si alloy		
y in Li_y–M	0.4	1.0	2.6	3.5	4.4	1.7	2.3	3.3
Redox potential V/V [vs. Li/Li^+]	0.78	0.69	0.4 4	0.44	0.43	0.58	0.43	0.4

The final resistance values were at least one order of magnitude greater than the values in the initial state. These results suggest that continuous SEI growth occurred during the cycling until the symmetric cells were essentially destroyed. The SEI resistan ce values of the cells in the initial state and following the 20th cycle are summarized in Table 1, confirming a clear relationship between the solid electrolyte composition and the growth rate of the SEI resistance. Increasing the germanium proportion evid ently accelerated the growth rate of the SEI resistance, indicating that the electrochemical reduction of germanium could con-tribute to decomposition of the solid electrolyte during the battery. Be-cause metals can be reduced and/or oxidized more readily than phosphorus, the decomposition of electrolytes containing larger amount of metals is one reason for the increases in both the SEI resistance and thickness. Since the SEI resistance increases during the charge–discharge reaction when employing LGPSx-based electrolytes, the SEI formation and growth might therefore be dependent on the electrochemical stability of the solid electrolyte.

3.2. EFFECTS OF ELECTRODE MATERIALS.

In order to obtain further information concerning the SEI formation process and the resistivity changes during cycling, the effects of the electrode composition were examined by varying the Li/M (M = Sn, Si) ratios in the electrodes. The Li/M ratios examined in the present study are summarized in Table 2, where the redox potentials of the electrodes are indicated for various lithium contents (y in Li_yM) [14,15]. Fig. 3 shows the SEI resistance values of cells incorporating Li_yM electrodes with three different LGPSx compositions following 20 cycles. Here the SEI resistances are plotted as functions of the reduction–oxidation (redox) potentials (vs. Li/Li^+) of the Li_yM alloys (Vr). The Vr potential depends on the lithium proportion in the alloys (lower y = higher Vr potential) and therefore the Vr value of an alloy $Li_{y+z}M$ (where y is the initial Li amount and z is the amount of Li (de)intercalated during electrochemical testing) can vary during the charge–discharge reactions. However, changes in the lithium content with the battery reaction in these symmetrical cells remained within the range defined by z = ±0.003, demonstrating that the potential changes of the electrodes during the charge–discharge cycles were negligible. Therefore, the Vr values for the electrodes are plotted using Vr for the initial y value.

Table 1

Composition dependence of R_{SEI} prior to cycling and following 20 cycles, and growth rates for the $Li_{4.4}Sn$ LGPSx/$Li_{4.4}Sn$ system.

	R_{SEI} prior to cycling	R_{SEI} following 20 cycles	R_{SEI} growth rate	Ge ratio in composition
LGPS0.5	48 Ω	1217 Ω	2535%	5.9%
LGPS0.65	41 Ω	458 Ω	1117%	4.2%
LGPS0.75	160 Ω	218 Ω	136%	3.0%

In the case of the Li_y–Sn electrode, the SEI resistances decreased with higher Vr values, indicating that an alloy electrode having a higher Vr resulted in a thin SEI layer at the electrode/electrolyte interface. This result is in good agreement with the finding that reduction of germanium in-creases the SEI resistance. Kim et al. have reported that GeS_2 exhibits a reduction reaction at potentials below 0.5 V (vs. Li/Li^+), and so a Vr value below 0.5 V was sufficient to form thicker SEI layer [16]. These data also confirmed that a higher ratio of germanium in the electrolyte generates increased SEI resistance, especially in the LGPS0.5 system. The SEI resistance in the cell using LGPS0.5 increases over the entire potential range, though it decreases with higher Vr values. Although there were slight differences in the absolute values of the SEI resistance be-tween the Li_y–Sn and Li_y–Si electrodes, both electrodes showed almost equivalent trends. The Li_y–Si electrodes with Vr values below 0.5 V in-creased the SEI resistivity, while the cell incorporating LGPS0.5 exhibit-ed the highest resistivity at 1294 Ω after final cycling.

These results provide clear evidence that a lower Vr value enhances the reduction of germanium in LGPSx, which in turn triggers the decomposition of the solid electrolyte and increases the impedance of the SEI layer. In addition, the observed threshold potential of approximately 0.5 V also suggests that the reduction of germanium is the dominant factor in the formation and growth of the SEI layer during the battery reaction.

3.3. OBSERVATIONS OF THE ELECTROLYTE/ELECTRODE INTERFACE.

The SEI layer formed during the charge–discharge process was characterized by XRD analyses assessing the surfaces of specimens taken from cells following 20 cycles. To elucidate the relationship between the resistance and the SEI structure, two battery systems were selected: $Li_{3.5}Sn$ alloy/LGPS0.5/$Li_{3.5}Sn$ alloy and $Li_{3.5}Sn$ alloy/LGPS0.75/$Li_{3.5}Sn$ alloy, which had shown SEI resistance values of 1748 and 382 Ω after 20 cycles, respectively. A reaction at the interfacial region was suggested by a change in the color of the electrolyte surface from gray-yellow to dark-gray for both electrolytes after 20 cycles. Fig. 4 provides the XRD patterns of the LGPS0.5 and LGPS0.75 specimens in the as-prepared state and following electrochemical cycling. After 20 cycles, the $Li_{3.5}Sn$/LGPS0.5 interface produced clear diffraction peaks originating from an unknown phase, while the diffraction peaks due to the LGPS0.5 had largely disappeared. This specimen corresponds to the highest resistivity in the tested batteries, indicating destruction of the cell during cycling. In the case of the $Li_{3.5}Sn$/LGPS0.75 interface, diffraction peaks from an unknown phase were also observed due to a decomposition product of the electrolyte. However, the intensities of these unknown phase peaks relative to those of the original LGPS0.75 were quite small. This result demonstrates that the LGPS0.75 possesses great-er electrochemical stability than the LGPS0.5 due to its lower germanium content. These data show that the lower germanium contents in the solid electrolyte could provide a suitable electrochemical reaction field for battery reactions. Ex situ XRD measurements therefore con-firmed the decomposition rate of the solid electrolyte and its compositional variation during the battery reactions. In addition, partial decomposition of the LGPS0.75 revealed the formation of an electro-chemically stable thin SEI layer.

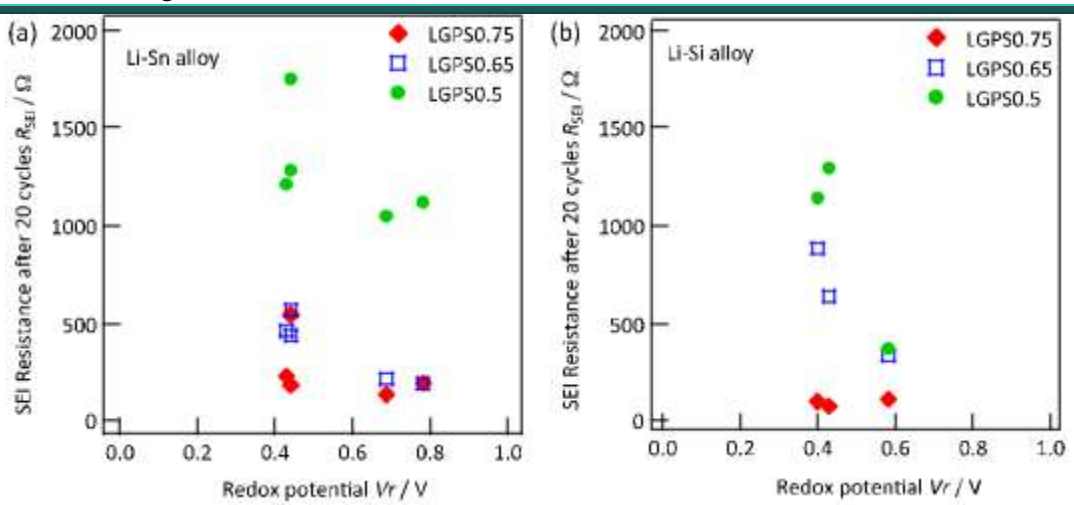

Fig. 3. Relationship between the SEI resistance of LiSn alloy/SE/LiSn alloy cells (SE: solid electrolyte) following 20 cycles and Vr, where Vr is the redox potential of the electrode.

In order to evaluate changes in the elemental distribution in the electrolyte with cycling, EDX elemental analysis was carried out on a cross-section of the interface of a $Li_{3.5}Sn$ alloy/LGPS0.5/$Li_{3.5}Sn$ alloy cell, both in its initial state and after 20 cycles. Fig. 5 shows the cross-sectional SEM images of electrolytes removing the electrode (a) initial, after 20th cycle. EDX elemental analyses were carried out within a range of 10 µm from electrode/electrolyte interface. The EDX line analyses were carried out along the red line seen in the SEM images. Anode electrodes had been removed from the electrolyte before the SEM and EDX measurements. Fig. 6 shows the changes in the elemental distribution in the electrolyte along the depth direction from the electrode/electrolyte interface to the electrolyte bulk. Phosphorus and sulfur levels are seen increasing over a 1 µm range from the surface region with electrochemical cycling while germanium decreased at the interface, indicating changes in the elemental distribution associated with formation of the SEI.

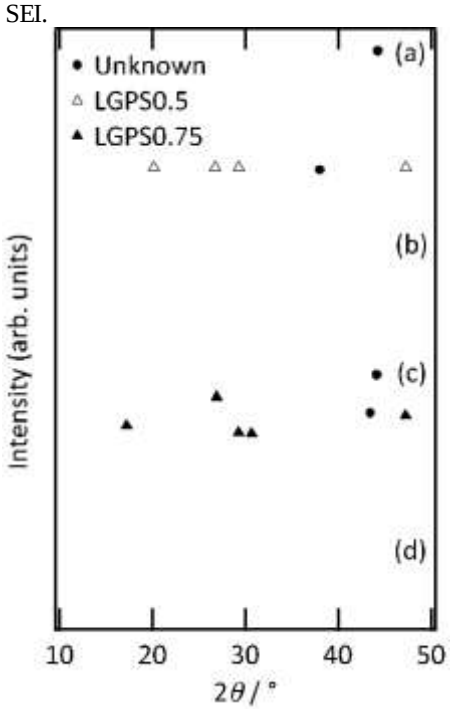

Since Kim et al. reported that a reduction of GeS_2 electrode generates Li_2S and Ge–Li alloy [16], a hypothesis could be that a reduction of the LGPS electrolytes provides three components, a Ge–Li alloy on the anode surface, possibly removed by the anode pealing process, Li_2S and Li–P–S materials at the electrolyte surface. These interfacial changes over a 1 µm range and the accompanying electrolyte decomposition might contribute to higher SEI resistance values.

To assess the SEI composition effects on resistance, charge–dis-charge measurements were carried out with artificial additives at the $Li_{0.4}Sn$/LGPS0.5 interface. Three materials were selected as additives: Li_2S (Nihon Kagaku Kogyo), GeS_2 (Kojundo Chemical Laboratory, 99.9% N purity) and P_2S_5 (Aldrich, 99.9% N purity). These additives all represent raw ingredients for the

synthesis of LGPSx, and thus could be expected to be present at the interface after decomposition reactions due to the SEI formation. The process by which these new cells were fabricated was essentially the same as that used to produce the earlier, non-additive cells.

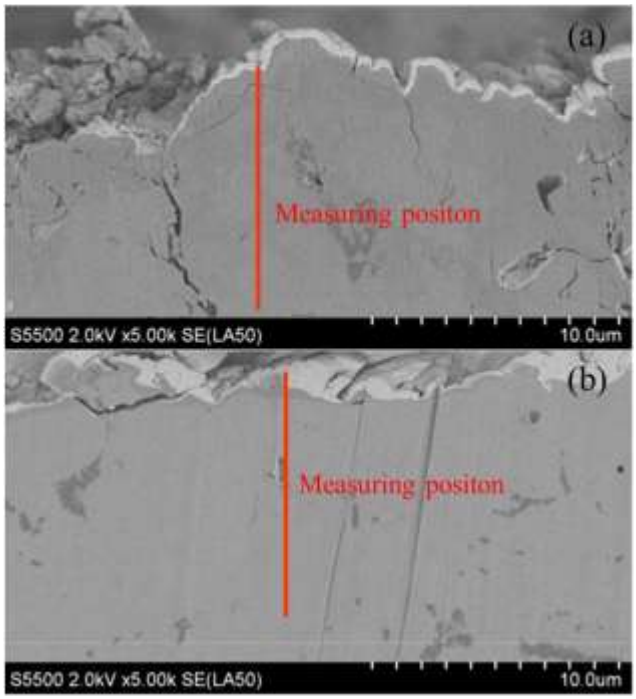

Fig. 4. XRD patterns of the solid electrolytes: (a) the electrode/electrolyte interface of the $Li_{3.5}Sn$ alloy/LGPS0.5/$Li_{3.5}Sn$ alloy cell after 20 cycles, (b) as-prepared LGPS0.5, (c) the $Li_{3.5}Sn$ alloy/LGPS0.5/$Li_{3.5}Sn$ $Li_{3.5}Sn$ alloy/LGPS0.75/$Li_{3.5}Sn$ alloy cell after 20 cycles and (d) as-prepared LGPS0.75.

Fig. 5. SEM image of the cross-sectional electrolyte sample of $Li_{3.5}Sn$ alloy/LGPS0.5/$Li_{3.5}Sn$ alloy cell, (a) before cycling and (b) after 20 cycles.

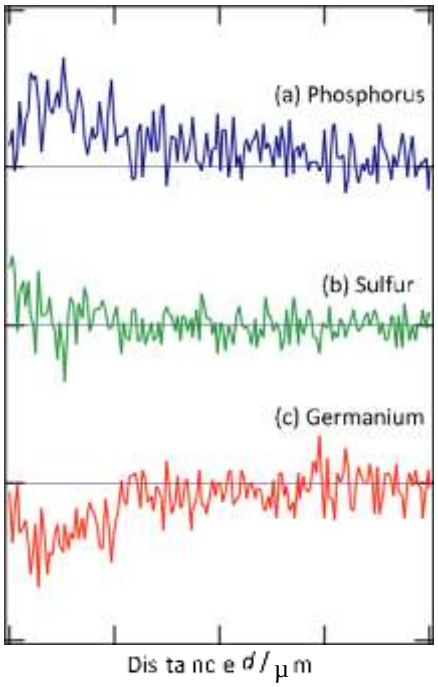

Fig. 6. Changes in the element distribution along the depth direction for a cross-section following 20 cycles by EDX elemental analysis for a $Li_{3.5}Sn$ alloy/LGPS0.5/$Li_{3.5}Sn$ alloy cell.

Approximately 1 mg of the desired additive in pow-der form was added to the electrolyte pellet, distributed over one side, after which the pellet was pressed at 184 MPa and a $Li_{0.4}Sn$ electrode was subsequently pressed onto the additive material layer. The

other side of the specimen was constructed in the same manner so as to maintain symmetry. Fig. 7 shows the variations of the SEI resistances of these symmetric cells incorporating additives upon cycling. The initial SEI resistances of the cells with additives were comparable to that of the non-additive cell, indicating that the additives did not affect the initial impedance at the interface remarkably; non-additive = 28 Ω, and with-additives P_2S_5 = 97 Ω, Li_2S = 70 Ω, GeS_2 =17Ω.

The SEI resistances of all cells increased with cycling, and it is note-worthy that there was a clear difference in the SEI resistance growth rates.

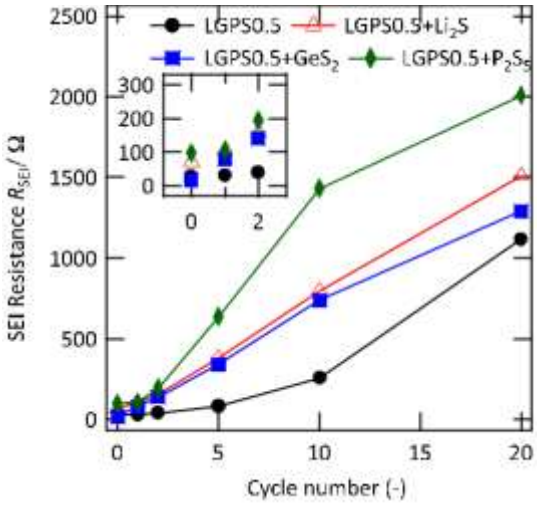

Fig. 7. Cycling dependence of the SEI resistance for cells with added Li_2S, GeS_2 and P_2S_5 at the $Li_{0.4}Sn$ alloy/LGPS0.5 interface.

The SEI resistances increased to 2009 and 1511 Ω when incorporating the additives P_2S_5 and Li_2S, respectively. Conversely, the cell with GeS_2 as an additive showed comparable resistance to that of the non-additive cell; non-additive = 1119 Ω and with-additives GeS_2 = 1291 Ω. Following 20 cycles, the SEI resistance of the cell to which P_2S_5 has been added at the electrode/electrolyte interface was the highest of the four cells. This result indicated that P_2S_5 additive reacted with Li_2S and/or Li-ion at the interface, and this reaction could contribute to further Li–P–S compounds formation. Thus, the presence of Li–P– S phases at the electrode/electrolyte interface generated by the decomposition of the LGPSx solid electrolyte is expected to increase the SEI resistance. In addition, P_2S_5 might increase the growth rate of the Li–P–S phases by the reaction with Li_2S and enhance continuous decomposition reaction at the interface.

4. CONCLUSION.

The stability of the electrode and electrolyte interface was studied in all-solid-state batteries with sulfide-based solid electrolytes. The results obtained in the present study may be summarized as follows.

(i) The solid electrolytes of the composition $Li_{4-x}Ge_{1-x}P_xS_4$ with smaller x value contribute to a thicker SEI formation due to the instability of the Ge in the LGPS structure during battery reactions.

(ii) Smaller interfacial resistances were observed for cells using Li–M (M = Sn, Si) alloy electrodes with higher redox potentials (vs. Li/ Li^+).

(iii) The composition of the SEI layer is an Li–P–S compound generated by electrolyte decomposition at the electrode/electrolyte interface and could be responsible for the observed increase in resistance.

The formation of the SEI layer at the electrode/electrolyte interface is an important factor in stabilizing the charge–discharge reactions in cells incorporating sulfide-based solid electrolytes. The optimization of the interface by the appropriate choice of electrode and electrolyte materials is important for the future development of all-solid-state batteries.

REFERENCES

[1] J.M. Tarascon, M. Armand, Nature 414 (6861) (2001) 359.
[2] M. Armand, J.M. Tarascon, Nature 451 (7179) (2008) 652.
[3] N. Kamaya, K. Homma, Y. Yamakawa, M. Hirayama, R. Kanno, M. Yonemura, T. Kamiyama, Y. Kato, S. Hama, K. Kawamoto, A. Mitsui, Nat. Mater. 10 (9) (2011) 682.
[4] T. Inada, T. Kobayashi, N. Sonoyama, A. Yamada, S. Kondo, M. Nagao, R. Kanno, J. Power Sources 194 (2) (2009) 1085.
[5] T. Kobayashi, A. Yamada, R. Kanno, Electrochim. Acta 53 (15) (2008) 5045.
[6] R. Kanno, M. Murayama, T. Inada, T. Kobayashi, K. Sakamoto, N. Sonoyama, A. Yamada, S. Kondo, Electrochem. Solid-State Lett. 7 (12) (2004) A455.

[7] O. Kwon, M. Hirayama, K. Suzuki, Y. Kato, T. Saito, M. Yonemura, T. Kamiyama, R. Kanno, J. Mater. Chem. A 3 (1) (2015) 438.
[8] C. Wang, A. John Appleby, F.E. Little, J. Power Sources 93 (1–2) (2001) 174.
[9] R.A. Huggins, J. Power Sources 81–82 (1999) 13.
[10] R.Z. Hu, L. Zhang, X. Liu, M.Q. Zeng, M. Zhu, Electrochem. Commun. 10 (7) (2008) 1109.
[11] R. Kanno, M. Murayama, J. Electrochem. Soc. 148 (7) (2001) A742.
[12] Scriner Associates Inc., North Carolina, USA, 1998.
[13] T. Sakai, Electrochemistry 71 (8) (2003) 722.
[14] K. Hirai, T. Ichitsubo, T. Uda, A. Miyazaki, S. Yagi, E. Matsubara, Acta Mater. 56 (7) (2008) 1539.
[15] W.J. Weydanz, M. Wohlfahrt-Mehrens, R.A. Huggins, J. Power Sources 81–82 (1999) 237.
[16] Y. Kim, H. Hwang, K. Lawler, S.W. Martin, J. Cho, Electrochim. Acta 53 (15) (2008) 5058.